Aeromechanical Stability Analysis and Control of Smart Composite Rotor Blades

ADITI CHATTOPADHYAY
JONG-SUN KIM
QIANG LIU
Department of Mechanical and Aerospace Engineering, Arizona State University, Tempe, AZ 85287-6106, USA

Abstract: The use of segmented constrained layer damping treatment and closed loop control is investigated for improved rotor aeromechanical stability. The rotor blade load-carrying member is modeled using a composite box beam with arbitrary wall thickness. The ACLs are bonded to the upper and lower surfaces of the box beam to provide active and passive damping in the aeromechanical stability analysis. A finite element model based on a hybrid displacement theory is used to accurately capture the transverse shear effects in the composite primary structure, the viscoelastic and the piezoelectric layers within the ACL. The Pitt-Peters dynamic inflow model is used in the air resonance analysis under hover conditions. Rigid body pitch and roll degrees of freedom and fundamental flap and lead-lag modes are considered in this analysis. A transformation matrix is introduced to transform the time-variant system to a time-invariant system. A LQG controller is designed for the transformed system based on the available measurement output. The control performance is compared with the results of the open loop and the passive control systems. Numerical results indicate that the proposed control system with surface bonded ACL damping treatment significantly increases rotor lead-lag regressive modal damping in the coupled rotor-body system.

Key words: Helicopter aeromechanical stability, smart material, robust control

1. INTRODUCTION

Helicopter aeromechanical stability analysis is a key issue in rotor design. Current rotor designs tend towards hingeless and bearingless configurations, which are often soft-inplane due to stress and weight considerations. These rotor systems are more susceptible to aeromechanical instabilities such as ground and air resonance instabilities due to the interaction of the poorly damped regressing lag mode and body mode. In general for a helicopter in operation, the lead-lag modes tend to diverge without enough rotor mechanical damping. Therefore, increase of lead-lag damping in rotor blades has been investigated for many years, in order to improve helicopter aeroelastic and aeromechanical stability. Recent research has shown that improvements in helicopter vibration reduction, aeroelastic stability and aeromechanical stability can be achieved by using smart materials and active control techniques. Elastomeric dampers have received a significant amount of attention (McGuire, 1994) due to the variety of advantages they exhibit over conventional dampers. However, these dampers are sensitive to temperature, exhibiting significant loss of damping at extreme temperatures, and have been known to cause limit cycle oscillations in rotor blades. A numerical study of electrorheological (ER) dampers was conducted by Kamath and Wereley

Journal of Vibration and Control, **8:** 847–860, 2002 DOI: 10.1177/1077546029187

(1995). The feasibility of using magnetorheological fluid-based dampers for lag damping augmentation in helicopters was addressed in their paper. A new form of active constrained layer (ACL) with edge element, known as EACL, was used in the flex beam of helicopter rotor blade to improve aeromechanical stability (Badre-Alam, Wang and Gandhi, 1999). More recently, the use of ACL damping treatment for passive augmentation of ground and air resonance stability was investigated by Liu et al. (2000). The study indicates that significant improvement in lead lag damping can be achieved through the use of this type of damping treatment.

The concept of active constrained layer (ACL) damping treatment has been investigated by many researchers in the context of vibration control (Baz and Ro, 1993; Ro and Baz, 1996). An ACL configuration comprises a piezoelectric layer and a viscoelastic bonding layer that connects the piezoelectric layer to the surface of the primary structure. The piezoelectric layers have sensing and control capabilities that actively tune the shear of the viscoelastic layer based on the structural response. Thus the energy dissipation mechanism of the viscoelastic layer is enhanced and the damping characteristic of the host structure can be improved. The segmented configuration in the active constrained layer damping treatment was explored by Lesieutre and Lee (1996). It was found that segmentation provided the possibility of additional independent control inputs to improve the structural performance.

It is well known that a segmented active constraining layer is an effective means of increasing passive damping in low frequency vibration modes by increasing the number of high shear regions. A more comprehensive and practical approach to model sparse sequenced ACL damping treatment on composite plates of arbitrary thickness was recently developed by Chattopadhyay et al. (2001). In this work, a hybrid displacement theory was developed to efficiently model the transverse shear stresses in the various layers. Since the ACL configuration capitalizes on both passive and active damping techniques in a synergistic manner, it has been shown to be an effective method for vibration suppression in composite structures. Recently, this concept was extended for rotary wing applications (Badre-Alam, Wang and Gandhi, 1999; Liu et al., 2000). The segmented constrained layer (SCL) configuration was used by Liu et al. (2000) to investigate improvement in passive inplane damping in rotor blades; no active control technique was employed.

The objective of this paper is to extend the above work using active control methodology. The goal is to investigate the active damping of a smart rotor blade, built around a composite box beam, with segmented active constrained layer damping treatment. An air resonance model is used to investigate the coupled rotor-body stability. For rotary wing applications, the controller must be designed so as to deal with the time-variant characteristics of the dynamic model due to rotor rotation. Since the obtained open loop model is time-variant, it is difficult to apply the well developed linear control methods. In this work, a transformation matrix is used to transform the time-variant problem to a time-invariant problem. A linear quadratic Gaussian (LQG) controller is then designed based on the linear time-invariant model. Numerical studies conducted show that the proposed control system is effective in improving helicopter aeromechanical stability over a wide range of operating speed.

2. STRUCTURAL MODELING

A composite box beam model of arbitrary wall thickness is used to present the principal rotor load-carrying member in rotor blades. Segmented ACLs are surface bonded to the top and

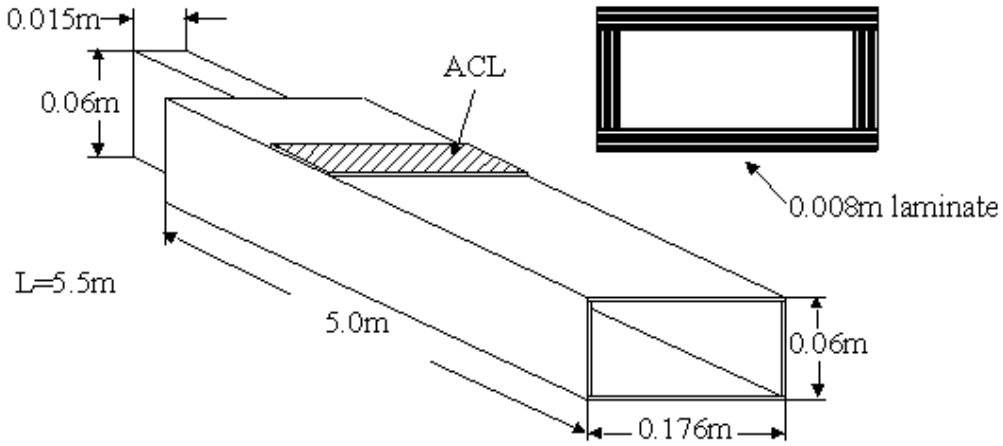

Figure 1. Configuration of composite box beam with ACLs.

bottom surfaces of the box beam (Figure 1). Since an ACL consists of a piezoelectric layer and a viscoelastic bonding layer, it is necessary to accurately model the displacement fields in the various regions and incorporate boundary and the continuity conditions between the different layers. A new hybrid displacement theory was recently developed by Chattopadhyay et al. (2001) to model surface bonded ACL on a composite plate. The theory uses a higher order displacement field to capture the significant transverse shear effects in the composite primary structure. Since viscoelastic and piezoelectric layers are made from isotropic material, the first and the second order displacement fields are employed in these layers to maintain computational efficiency. The refined displacement fields, defined in the three different material layers, are derived by applying the displacement and transverse shear stress continuity conditions at the layer interfaces, and the traction-free boundary conditions on the top and the bottom surfaces of the structure. This plate model was then extended to develop a finite element model for the analysis of the composite box beam with surface bonded ACL damping treatment by Liu et al. (2000). A brief description of the model is presented for complete understanding.

The box beam is modeled using composite laminates representing the four walls (Figure 2). In the hybrid displacement theory, each wall of the box beam is separated through the thickness into three different regions. These are: composite region (region *c*), viscoelastic region (region *v*) and piezoelectric region (region *p*). The following refined displacement field is obtained after satisfaction of the stress-free boundary conditions at the free surfaces:

$$
\begin{aligned}
u^c &= u_0^c - z w_{0,x}^c + z\left(1 - \frac{4z^2}{3h^2}\right)\psi_x^c + \frac{2z^2}{3h^2}\left(z + \frac{3}{4}h\right)\frac{G^v}{G_{13}^c}\psi_x^v \\
v^c &= v_0^c - z w_{0,y}^c + z\left(1 - \frac{4z^2}{3h^2}\right)\psi_y^c + \frac{2z^2}{3h^2}\left(z + \frac{3}{4}h\right)\frac{G^v}{G_{23}^c}\psi_y^v
\end{aligned}
\tag{1a}
$$

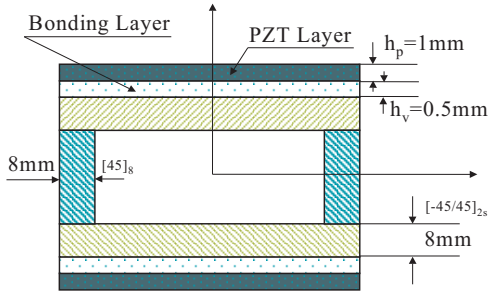

Figure 2. Illustration of box beam element and walls with ACLs.

$$
\begin{aligned}
w^c &= w_0^c \quad \text{where } -\frac{h}{2} \le z \le \frac{h}{2} \\
u^v &= u_0^c + \frac{h}{3}\psi_x^c - z w_{0,x}^c + \left(z - \frac{h}{2} + \frac{5h}{24}\frac{G^v}{G_{13}^c}\right)\psi_x^v \\
v^v &= v_0^c + \frac{h}{3}\psi_y^c - z w_{0,y}^c + \left(z - \frac{h}{2} + \frac{5h}{24}\frac{G^v}{G_{23}^c}\right)\psi_y^v \qquad \text{(1b)} \\
w^v &= w_0^c \quad \text{where } \frac{h}{2} \le z \le \frac{h}{2} + h_v \\
u^p &= u_0^c + \frac{h}{3}\psi_x^c - z w_{0,x}^c \\
&+ \left(\frac{G^v}{G^p}\frac{1}{2h_p}\left(2h_4 z - z^2 - h_3 h_4 - h_3 h_p\right) + h_v + \frac{5h}{24}\frac{G^v}{G_{13}^c}\right)\psi_x^v \\
v^p &= v_0^c + \frac{h}{3}\psi_y^c - z w_{0,y}^c \\
&+ \left(\frac{G^v}{G^p}\frac{1}{2h_p}\left(2h_4 z - z^2 - h_3 h_4 - h_3 h_p\right) + h_v + \frac{5h}{24}\frac{G^v}{G_{23}^c}\right)\psi_y^v \qquad \text{(1c)} \\
w^p &= w_0^c \quad \text{where } \frac{h}{2} + h_v \le z \le \frac{h}{2} + h_v + h_p
\end{aligned}
$$

with

$$
h_3 = \frac{h}{2} + h_v, \quad h_4 = \frac{h}{2} + h_v + h_p \qquad (2)
$$

where u, v and w are the inplane and the out of plane displacements at a point (x, y, z), u_0, v_0 and w_0 represent the displacements at the midplane, and ψ_x and ψ_y represent the rotations of the normals to the midplane. The quantity G is the shear modulus of the material. The present approach is capable of capturing the varying behaviors in the different material regions while being computationally efficient.

The continuity conditions at the section interface require that the displacements defined in an adjacent section (equation (1)) be equal to each other through the thickness. These lead to the following conditions:

$$\psi_x^v(x,y) = \psi_y^v(x,y) = 0, \quad (x,y) \in \Gamma_s \tag{3}$$

where Γ_s represents the section interface.

For a wall with segmented viscoelastic layer and piezoelectric constraining layer, the anelastic displacement field method (Chattopadhyay et al., 2001) is used to implement the viscoelastic material model. This enables time domain finite element analysis. For the wall with ACL, the total displacement vector (u) is divided into two parts, the discretized displacement vector (u_g), which represents the wall displacement including the composite, the viscoelastic and the piezoelectric layers, and the anelastic displacement vector (u_v) pertaining to the viscoelastic layer, that is, $u = [u_g, u_v]^T$.

The equations of motion for the box beam element are derived by combining the four walls. Using Hamilton's principle, the governing equations are expressed as follows:

$$M_g \ddot{u}_g + K_g u_g - K_{gv} u_v = F_g \tag{4}$$

where M_g and K_g are the structural global mass and stiffness matrices, respectively, and K_{gv} is the additional structural global stiffness matrix due to the anelastic displacement vector (u_v). The quantity F_g is the external force.

An additional set of ordinary differential equation that describes the time evolution of the anelastic displacement field is employed to obtain the solution of the entire system,

$$\begin{bmatrix} M_g & 0 \\ 0 & 0 \end{bmatrix} \begin{Bmatrix} \ddot{u}_g \\ \ddot{u}_v \end{Bmatrix} + \begin{bmatrix} 0 & 0 \\ 0 & \dfrac{c}{\Omega_d} K_v \end{bmatrix} \begin{Bmatrix} \dot{u}_g \\ \dot{u}_v \end{Bmatrix}$$
$$+ \begin{bmatrix} K_g & -K_{gv} \\ -K_{gv}^T & cK_v \end{bmatrix} \begin{Bmatrix} u_g \\ u_v \end{Bmatrix} = \begin{Bmatrix} F_g \\ 0 \end{Bmatrix} \tag{5}$$

where K_v is the global stiffness matrix constituting anelastic strain, c is the material constitutive coupling parameter and Ω_d is the characteristic relaxation time at constant strain. The force boundary conditions are imposed to couple the box beam and viscoelastic bonding layer in time domain.

3. AIR RESONANCE ANALYSIS

The air resonance model is shown in Figure 3. Only rigid body pitch and roll rotation degrees of freedom are taken into account in this model. A fundamental flap modal displacement (β_k) and a fundamental lead-lag modal displacement (ξ_k) are considered. The blade pitch degree of freedom is not included in the analysis. In Figure 3, variables φ_x and φ_y represent fuselage roll and pitch displacements, respectively. The center of gravity (C.G) of the helicopter is in the rotor shaft and h denotes the distance from the C.G to the hub center. The variable ψ_k is the azimuth angle and Ω is the rotor rotational speed. Segmented ACLs are bonded on the top

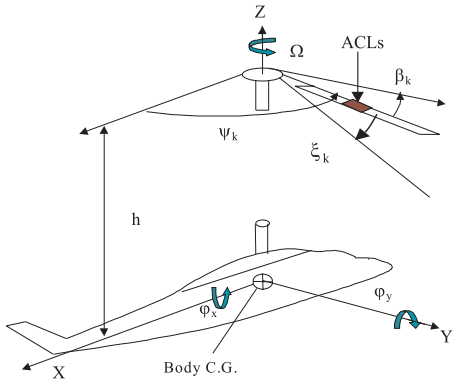

Figure 3. Air resonance model.

and bottom surfaces of the composite box beam, which represent the load-carrying member of the rotor blade.

It is assumed that the blade mass is distributed uniformly along the blade span and the planform is assumed to be rectangular. It is also assumed that there is no geometric twist. To further simplify the problem, it is assumed that there is no structural coupling between flap and lead-lag motions. The individual blade flap and lead-lag motions are combined together and are transferred to the non-rotating coordinate system through multiblade transformation. The modal damping of the box beam with ACLs is calculated in terms of equation (5) and is used in the blade flap and lead-lag equilibrium equations. In these equations, aerodynamic load is used as external force vector acting on the rotor blades.

The aerodynamic forces are calculated based on quasi-steady lifting line theory, combined with a dynamic inflow model. This model, due to Pitt and Peters (1981), can be expressed as follows:

$$v_1 = v_{1c}\bar{r}\cos\psi_k + v_{1s}\bar{r}\sin\psi_k \tag{6}$$

$$\begin{bmatrix} \frac{16}{45\pi} & 0 \\ 0 & \frac{16}{45\pi} \end{bmatrix} \begin{Bmatrix} \dot{v}_{1s} \\ \dot{v}_{1c} \end{Bmatrix} + \begin{bmatrix} v_s & 0 \\ 0 & v_s \end{bmatrix} \begin{Bmatrix} v_{1s} \\ v_{1c} \end{Bmatrix} = -\begin{Bmatrix} C_L \\ C_M \end{Bmatrix} \tag{7}$$

where v_1, v_{1c} and v_{1s} represent perturbations in the total, the cosine and the sine components of the induced velocity, respectively. The quantity $\bar{r}$ represents the blade radial station non-dimensionalized with respect to rotor radius. The quantities v_s and ψ_k denote dimensionless equilibrium velocity in hover and azimuth angles of the kth blade, and C_L and C_M are rolling and pitching moment coefficients, respectively.

The sectional lift (dF_z) and drag (dF_y) on the kth blade can be written as follows:

$$dF_z = \frac{1}{2}\rho\, ab\left(\theta\, U_T^2 - U_p U_T\right) dr$$

$$dF_y = -\frac{1}{2}\rho\, ab \left(C_d U_T^2 - \theta\, U_p U_T - U_p^2\right) dr \tag{8}$$

where a is the blade section lift-curve slope, b is the blade chord, θ is the collective pitch, and ρ is the air density. The quantities U_T and U_p are air velocities of blade section perpendicular and tangent to the disk plane, respectively. These can be expressed as follows:

$$\begin{aligned} U_T &= \Omega r - y' \\ U_p &= z' + v_0 + v_1 \end{aligned} \tag{9}$$

where v_0 is the reduced velocity of the rotor in equilibrium hover condition and z' and y' are flap and lead-lag velocities, respectively.

4. CONTROLLER DESIGN

4.1. Time-Variant Open Loop Model and Control Objective

It is important to examine the feasibility of eliminating the sinusoidal terms in the governing equations by using feedback control. Consider the linear time-variant system in state space form:

$$\begin{aligned} \dot{x}(t) &= Ax(\tau) + F(t)v(t) + Ew(t) \\ y(t) &= Cx(t) + n(t) \end{aligned} \tag{10}$$

where $x(t)$, $v(t)$ and $y(t)$ are the state, input and output vectors, respectively, and A, E and C are the system, disturbance and output matrices, respectively. The vector $x(t)$ consists of the two cyclic lead-lag angles and their time derivatives, two cyclic flap angles and their time derivatives, roll and pitch angles and their time derivatives, and two aerodynamic states. The control matrix $F(t)$ is periodic, that is $F(t) = F(t+\tau)$ with period $\tau = 2\pi/\Omega$, due to the rotating nature of the rotor blade with rotational speed Ω. It is assumed that six outputs are available, these are: two lead-lag angles, two flap angles and roll and pitch angles. A pair of ACL actuators is bonded to the top and bottom surfaces of the blade at the root of the four-bladed rotor. The disturbance $w(t)$ and the sensor noise $n(t)$ are both assumed to be stationary, having zero mean, uncorrelated with each other, Gaussian white, and to have covariance matrices satisfying

$$\begin{aligned} E\{w(t_1)w'(t_2)\} &= W\delta(t_1 - t_2) \\ E\{n(t_1)n'(t_2)\} &= N\delta(t_1 - t_2) \\ E\{w(t_1)n'(t_2)\} &= 0. \end{aligned} \tag{11}$$

In equation (11), the operator $E\{\}$ denotes the expected value, δ denotes the Kronecker delta, $(')$ denotes transpose and W and N represent intensities of the disturbance and the sensor noise, respectively. The control problem is to find the output feedback control input $v(t)$ in terms of output $y(t)$ so as to minimize the performance index, J_c,

$$J_c = E\left(\lim_{T\to\infty}\frac{1}{T}\int_0^T [\,x'(t)Qx(t) + \rho\, v'(t)v(t)]\,dt\right) \tag{12}$$

where Q is symmetric and positive semi-definite and ρ is a positive scalar. The weighting matrix Q is chosen as a diagonal matrix with larger weights for the lead-lag modes compared to the other modes.

4.2. Transformation To Time-Invariant System And LQG Control

The optimal control problem involves the solution of the time-varying Riccati equation (Nitzsche, 1994), which is not easy to calculate over the entire operation period. Moreover, since the resulting closed loop system is time-variant, it is difficult to utilize well-known physical parameters such as natural frequency and damping ratio. In this research, a transformation matrix is used to transform the time-variant system to the time-invariant system. The transformation matrix is defined as

$$v(t) = G(t)u(t) \tag{13}$$

where the transformation matrix $G(t)$ satisfies the relation $F(t)G(t) = B$, where B is time invariant and $G(t)$ is unitary, that is, $G'(t)G(t) = I$.

Substitution of equation (13) into equations (10) and (12) yields the following linear time-invariant control design problem:

$$\begin{aligned} \dot{x}(t) &= Ax(t) + Bu(t) + Ew(t) \\ y(t) &= Cx(t) + n(t) \end{aligned} \tag{14}$$

and

$$J_c = E\left(\lim_{T\to\infty}\frac{1}{T}\int_0^T [\,x'(t)Qx(t) + \rho\, u'(t)u(t)]\,dt\right). \tag{15}$$

The output feedback controller based on the linear quadratic Gaussian (LQG) method has the following form:

$$\begin{aligned} \dot{\hat{x}}\,(t) &= A\hat{x}(t) + Bu(t) + H[\,y(t) - C\hat{x}(t)] \\ y(t) &= -K\hat{x}(t) \end{aligned} \tag{16}$$

where $\hat{x}(t)$ is the estimated value of $x(t)$. The control gain matrix K and filter gain matrix H are determined from the linear quadratic control theory and the Kalman filter theory, respectively. The matrices K and H are obtained from two algebraic Riccati equations: the control algebraic Riccati equation (CARE) and filter algebraic Riccati equation (FARE) [12]. This is explained as follows:

$$\begin{aligned} K &= \frac{1}{\rho}B'P \\ PA + A'P - \frac{1}{\rho}PBB'P + Q &= 0 \quad \text{(CARE)} \end{aligned} \tag{17}$$

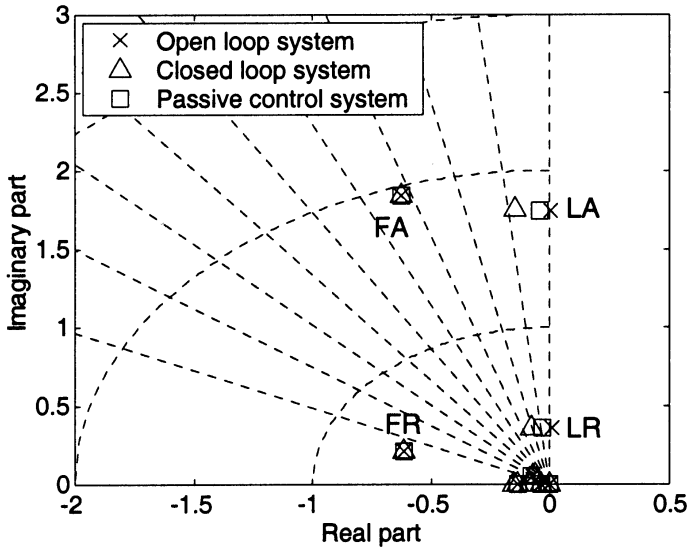

Figure 4. Poles of open and closed loop systems.

$$H = SC'N^{-1}$$

$$SA' + AS - SC'N^{-1}CS + EWE' = 0 \quad \text{(FARE)}.$$

The actual control input $v(t)$ can be obtained from

$$v(t) = G(t)u(t). \tag{18}$$

5. RESULTS AND DISCUSSION

The aeromechanical behavior of a rotor blade built around the composite box beam, with one pair of top and bottom surface bonded ACLs, is studied in detail. For the rotor-body coupled system investigated, the ratio of blade first mass moment to blade inertia (S_ξ/I_ξ) is 1.5. The dimensionless fuselage roll and pitch inertia are 2.86 and 9.42, respectively. For the four-bladed rotor studied, the rotor is assumed to operate at the normal angular velocity Ω_0 of 37.5 (rad/s) and with ± 25 percent variations. The fundamental flap and lead-lag frequency ratios of the rotor blade are $\varpi_\beta = 1.08$ and $\varpi_\xi = 0.62$ $(\Omega = \Omega_0)$, respectively. The blade airfoil profile lift-curve slope is 2π and drag coefficient is 0.01. The dimensionless distance from the fuselage center of gravity to the rotor plane (h/R) is 0.312 (Figure 3).

In Figure 4, the coupled rotor-body system poles are shown for the seven system modes $(\Omega = \Omega_0)$: lead-lag regressive mode (LR), lead-lag advancing mode (LA), flap regressive mode (FR), flap advancing mode (FA), gyroscopic mode (GS), dynamic inflow mode (DI) and zero root mode. The results are calculated for lock number $\gamma = 5$ and collective pitch $\theta = 0.15$. As shown in Figure 4 and Table 1, the open loop system is unstable without sufficient rotor mechanical lead-lag damping. The unstable modes are the LR and LA modes.

Table 1. Damping ratios of open and closed loop systems.

Mode	Open loop	Passive control	Active control
LR	-0.01895	0.07805	0.21694
LA	$-8.3242E-4$	0.02303	0.08508
FR	0.94754	0.94740	0.94738
FA	0.32284	0.32362	0.32094
GS	0.79994	0.80114	0.80193
DI	$-$	$-$	$-$

The LR mode is more unstable than the LA mode in this case. It is well known that lead-lag motion is associated with lower modal damping due to less aerodynamic loads. This can also be observed from Table 1, in which the values of two flap damping ratios are more than 0.3. With the application of active control methods to the coupled system, the closed loop system is stabilized. The modal damping ratios of 0.08508 for the LA mode and 0.21694 for the LR mode are obtained at rotor normal rotational speed. The lead-lag damping ratios of the closed loop system are much larger than the passive control system, which results in modal damping ratios of 0.02303 and 0.07805. This implies a 270 percent increase in damping for the LA mode and a 180 percent increase for the LR mode. To show the robustness of the proposed control scheme, the poles of the open loop and closed loop systems are calculated over a range of operating speed (± 25 percent) and are shown in Figures 5(a) and 5(b). While the relative stability of the lead-lag regressive mode become worse as the rotating speed increases (Figure 5(a)), it is seen that the closed loop system remains stable over 25 percent variations in rotating speed (Figure 5(b)).

Figure 6 shows the response when an impulsive force is exerted on the actuators. It is observed that the convergence of two cyclic flap responses is faster than the cyclic lead-lag responses due to the large damping ratios that are inherent to these modes. The cyclic lead-lag responses tend to damp out within 40 non-dimensional time (about 1 [s] in real time scale). The roll and pitch angles do not converge to zero due to the rigid body poles that are located at the origin, which are almost uncontrollable. Figure 7 shows the impulse response of the closed loop system at the different operating speeds. The proposed control system is sufficient to suppress the unstable lead-lag vibrations over a wide operating range. To examine the required control energy, the electric voltages for four pairs of actuators are also shown in Figures 8 and 9. The control input $u(t)$ as shown in Figure 8 is calculated based on the LQG control scheme and it has the same frequency component as the output. However, the actual control input $v(t)$ shown in Figure 9 has low frequency contents, in contrast to $u(t)$ and $y(t)$, due to the time-variant transformation matrix. Since the transformation matrix is unitary, the actual control input has the same quadratic norm as the calculated control input, which is within the practical voltage limit of piezoelectric actuators.

6. CONCLUSIONS

The use of a segmented active constrained layer (ACL) damping treatment on helicopter aeromechanical stability, particularly air resonance, has been investigated. The principal load-carrying member in the rotor blade is represented by a composite box beam with segmented constrained layers bonded on the top and bottom surfaces of the beam at the root

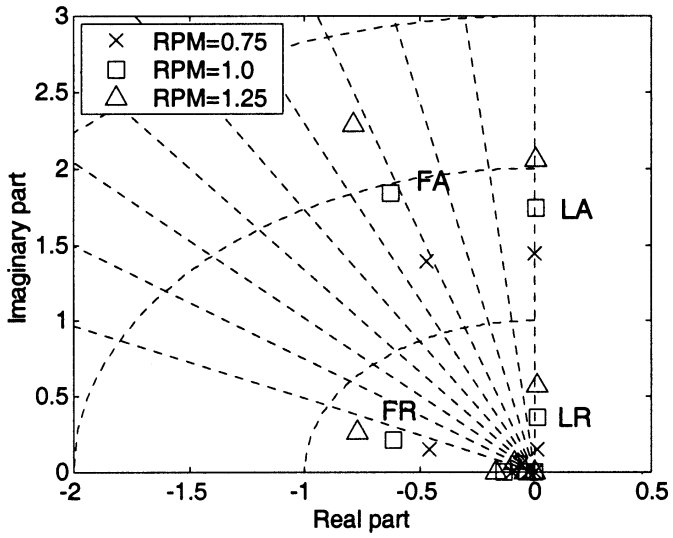

Figure 5(a). Root loci of open loop systems.

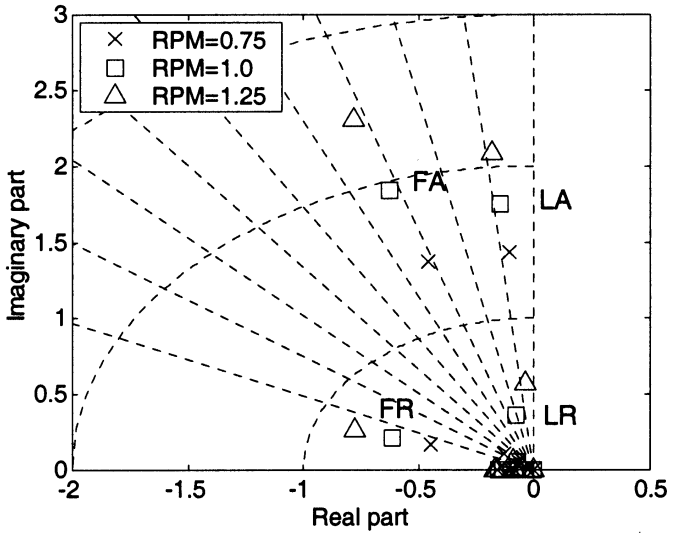

Figure 5(b). Root loci of closed loop systems.

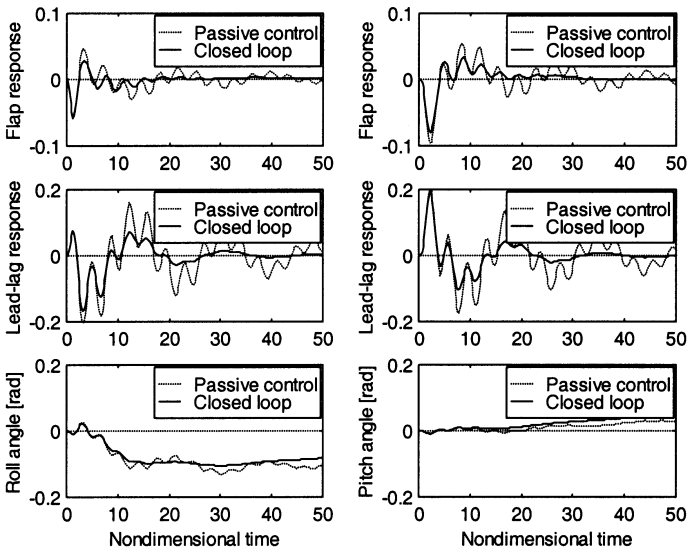

Figure 6. Response of the passive and active control systems.

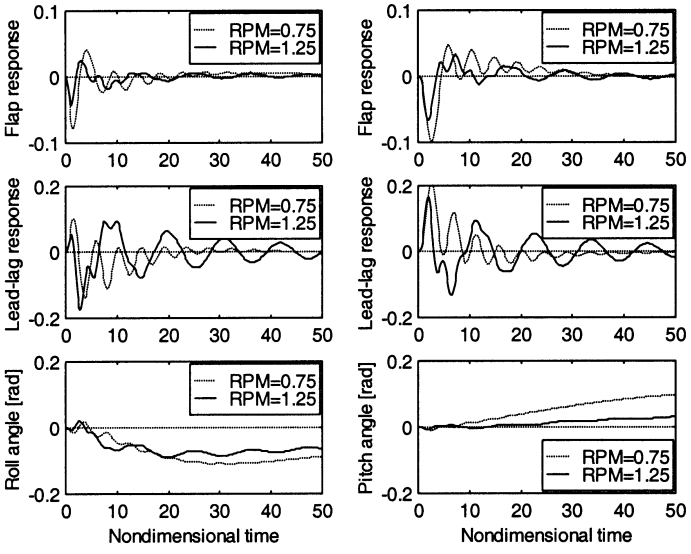

Figure 7. Response of the active control systems.

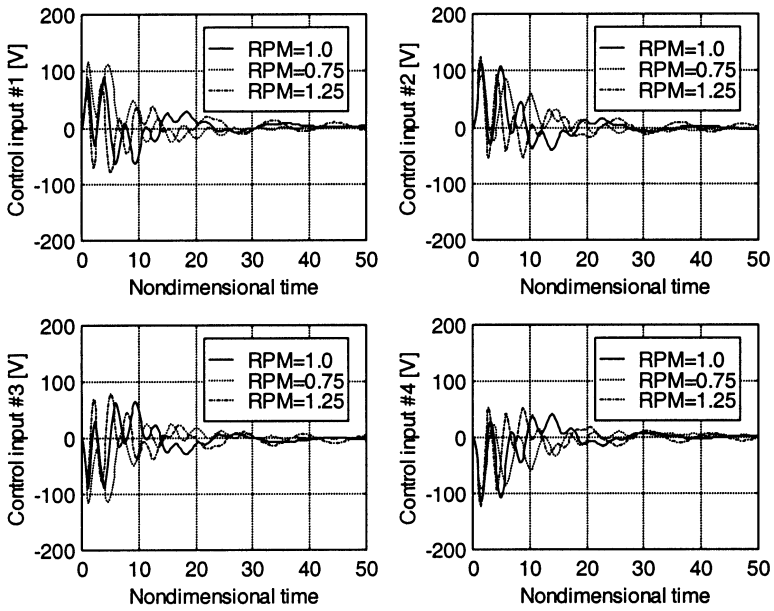

Figure 8. Calculated control input $[u(t)]$.

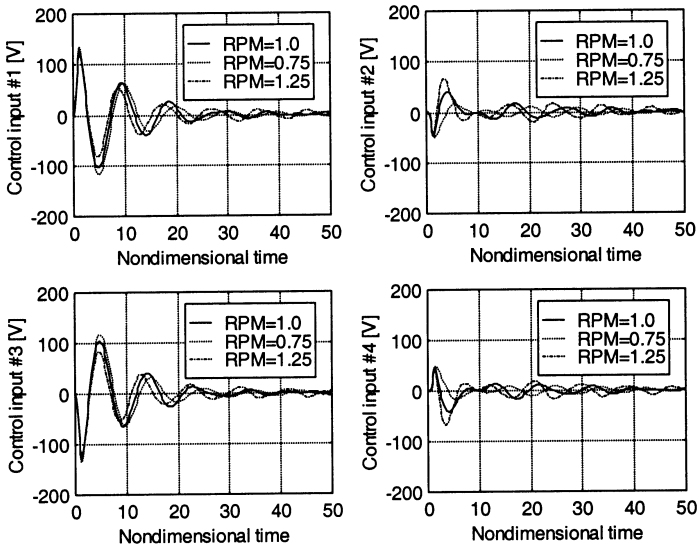

Figure 9. Actual control input voltages $[v(t)]$.

section. A finite element model is developed for the analysis of the smart box beam using hybrid displacement field theory. A LQG controller is designed based on the transformation matrix and its performance is compared with results of the open loop and the passive control systems. Numerical results indicate that the surface bonded ACLs with LQG control significantly increase rotor lead-lag regressive modal damping in the coupled rotor-body system. The following important observations are made from the present study.

(1) The use of a transformation matrix allows transformation of the time-variant system to a time-invariant system.
(2) The use of LQG control is efficient in stabilizing the unstable aeromechanical rotor response.
(3) The modal damping ratios obtained using closed loop control are significantly larger than the corresponding passive damping case.

Acknowledgment. The research was supported by the U.S. Army Research Office, grant number DAAH04-96-1-0163, technical monitor Dr. Gary Anderson.

REFERENCES

Badre-Alam A., Wang K.W., and Gandhi F., 1999, "Optimization of enhanced active constrained layer (EACL) treatment on helicopter flex beam for aeromechanical stability augmentation," *Journal of Smart Materials and Structures* **8**, 182–196.

Baz, A. and Ro, J., 1993, "Partial treatment of flexible beams with active constrained damping," in *Proceedings of Conference of the Society of Engineering Science* (ASME-AMD), Charlottesville, VA, Vol. 167, pp. 61–68.

Chattopadhyay, A., Gu, H., Beri R., and Nam, C., 2001, "Modeling segmented active constrained layer damping using hybrid displacement field," *AIAA Journal* **39**(3), 480–486.

Kamath, G.M. and Wereley N.M., 1995, "Development of ER-Fluid based actuators for rotorcraft flexbeam applications," in *Proceeding of SPIE's 2nd International Symposium on Smart Structures and Materials*, CA, February, Vol. 2443, pp. 120–133.

Lesieutre, G.A. and Lee, U., 1996, "A finite element for beams having segmented active constrained layers with frequency-dependent viscoelastics," *Journal of Smart Materials and Structures* **5**, 615–627.

Liu Q., Chattopadhyay, A., Gu, H., and Zhou, X., 2000, "Use of segmented constrained layer damping treatment for improved helicopter aeromechanical stability," *Journal of Smart Materials and Structures* **9**, 523–532.

McGuire, D.P., 1994, "Fluidlastic® dampers and isolators for vibration control in helicopters," in *Proceedings of the American Helicopter Society 50th Annual Forum*, Washington D.C., pp. 295–303.

Nitzsche, F., 1994, "Designing efficient blade controllers using smart structures," *AIAA-94-1766-CP.*

Pitt, D.M. and Peters, D.A., 1981, "Theoretical predictions of dynamic inflow derivatives," *Vertica* **5**(1), 3.

Ro, J. and Baz, A., 1996, "Optimum design and control of active constrained layer damping," *Journal of Mechanical Design and Journal of Vibration and Acoustics* (special combined edition) **117**, 135–144.

Stein, G. and Athans, M., 1978, "The LQG/LTR procedure for multivariable feedback control design," *Journal of IEEE Transactions on Automatic Control* **AC-32**, 105–114.